Biophysical Journal Volume 108 February 2015 957–966

Article

An Equilibrium Model for the Combined Effect of Macromolecular Crowding and Surface Adsorption on the Formation of Linear Protein Fibrils

Travis Hoppe[1] and Allen P. Minton[1,*]

[1]Section on Physical Biochemistry, Laboratory of Biochemistry and Genetics, National Institute of Diabetes and Digestive and Kidney Diseases, National Institutes of Health, Bethesda, Maryland

ABSTRACT The formation of linear protein fibrils has previously been shown to be enhanced by volume exclusion or crowding in the presence of a high concentration of chemically inert protein or polymer, and by adsorption to membrane surfaces. An equilibrium mesoscopic model for the combined effect of both crowding and adsorption upon the fibrillation of a dilute tracer protein is presented. The model exhibits behavior that differs qualitatively from that observed in the presence of crowding or adsorption alone. The model predicts that in a crowded solution, at critical values of the volume fraction of crowder or intrinsic energy of the tracer-wall interaction, the tracer protein will undergo an extremely cooperative transition—approaching a step function—from existence as a slightly self-associated species in solution to existence as a highly self-associated and completely adsorbed species. Criteria for a valid experimental test of these predictions are presented.

INTRODUCTION

The molecular mechanisms of a variety of biological phenomena, including cellular motility, mitosis, and prokaryotic cell division, involve the reversible formation of linear fibrils or fibers composed of globular protein subunits (e.g., actin, tubulin, and FtsZ) (1–3). The equilibria and kinetics of linear fiber formation under dilute solution conditions have been studied extensively both theoretically (4,5) and experimentally (2,3,6–9). The local environments within which protein fibrils are formed in vivo contain a high total concentration of soluble macromolecules that may interact nonspecifically with the fiber-forming protein, as well as a variety of relatively immobile structures, such as membranes or static filaments, that cumulatively present a large area of surface to which such fibers might adsorb reversibly (10,11). Both of these environmental factors have a potentially large effect on the equilibria and kinetics of fiber formation. Previous theoretical and experimental studies from our laboratory and others (12–14) have demonstrated that the tendency of a dilute protein to form fibrils is significantly enhanced in solutions containing high concentrations of nominally inert polymers and proteins, a phenomenon that is attributed primarily to excluded volume or macromolecular crowding (15–17). Other theoretical and experimental studies from our laboratory and others (18–20) have demonstrated that the presence of adsorbing surfaces can significantly enhance the tendency of dilute proteins to form adsorbed linear and nonlinear aggregates. For these reasons, we speculated that the presence of both high concentrations of inert macromolecules and surfaces to which the fiber-forming protein can adsorb might have a cumulative effect on fiber formation by the dilute protein that is greater than the sum of the separate effects of crowding and adsorption. This speculation motivated the development of the model presented below, which is intended to elucidate major energetic contributions to the overall process and therefore is mesoscopic rather than atomically detailed.

Description of the physical model

We introduce a highly simplified model for the combined effect of excluded volume and adsorption on protein fiber formation. The model consists of an enclosed solution of fixed volume that contains a variable total concentration of nonassociating molecules (termed crowder) and a fixed low total concentration of molecules (called tracer) that can self-associate to form indefinitely long linear fibrils. For simplicity, monomeric tracer and crowder are represented by spheres of radius r. Generalization to unequal sizes of crowder and tracer monomer is straightforward, but it increases the computational complexity without a correspondingly greater insight into fundamental processes. Fibrillar aggregates of tracer are represented by spherocylinders with a cylindrical radius r and a cylindrical length calculated such that the volume of an n-mer is equal to n times the volume

Submitted October 9, 2014, and accepted for publication December 17, 2014.

*Correspondence: minton@helix.nih.gov

Travis Hoppe's present address is Section on Theoretical Biophysical Chemistry, Laboratory of Chemical Physics, National Institute of Diabetes and Digestive and Kidney Diseases, National Institutes of Health, Bethesda, Maryland.

Editor: David Eliezer.

0006-3495/15/02/0957/10 $2.00

http://dx.doi.org/10.1016/j.bpj.2014.12.033

of monomer. With this condition, the ratio of the cylindrical length to the diameter of an n-mer, denoted by L_n, is equal to $2/3(n-1)$. The total volume of the system is partitioned into two compartments: the bulk compartment and a surface compartment adjacent to the hard wall enclosing the system. This compartment, which is taken to be planar on a molecular scale, has a thickness equal to $2Qr$, where Q is a factor that is only slightly larger than unity that is introduced to allow for the finite range of interaction between tracer and surface. Tracer particles lying entirely within this compartment are considered to be adsorbed. Crowder particles may accumulate within the surface compartment, but have no potential for interaction with the surface, whereas an adsorbed tracer n-mer within the surface compartment, lying approximately parallel to the plane of the surface, has a potential for interaction with the surface equal to $n\Delta H_{ads}/RT$. The ratio of the volume of the surface compartment to the total volume of the system is given by f_{surface}, which will vary with the total volume and shape of the system. The principal states of the system are depicted schematically in Fig. 1.

Equilibrium relations

Effect of crowding on fiber formation in bulk solution

The formation of fiber in solution is modeled by an isodesmic reaction scheme (8,21) in which the free energy of addition of a monomeric unit to the end (or ends) of a growing fiber is assumed to be independent of the length of the fiber for all n. It follows that the thermodynamic equilibrium constant for the addition of a monomer to an oligomer is given by

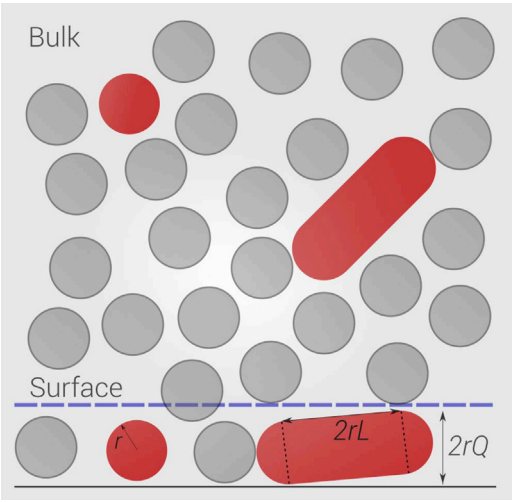

FIGURE 1 Principal states of the model system. Tracer species are depicted as red circles and spherocylinders, and crowder species are shown as gray circles. Upper left: tracer monomer in bulk; upper right: tracer n-mer in bulk; lower left, tracer monomer in the surface compartment; lower right: tracer n-mer in the surface compartment. To see this figure in color, go online.

$$K_0 = \frac{a_{b,n+1}}{a_{b,n}a_{b,1}}, \tag{1}$$

where $a_{b,i}$ denotes the thermodynamic activity of i-mer in the bulk fluid. We then define the apparent equilibrium constant

$$K \equiv \frac{c_{b,n+1}}{c_{b,n}c_{b,1}} = K_0\frac{\gamma_{b,n}\gamma_{b,1}}{\gamma_{b,n+1}} \tag{2}$$

or

$$\ln K = \ln K_0 + \ln \gamma_{b,1} + \ln \gamma_{b,n} - \ln \gamma_{b,n+1}, \tag{3}$$

where $c_{b,i}$ and $\gamma_{b,i}$ respectively denote the concentration and thermodynamic activity coefficient of species i in the bulk fluid. One can estimate the activity coefficient of each species present in the model system using results obtained from the scaled-particle theory of convex hard-particle fluids. In this instance, the logarithm of the activity coefficient of an isolated spherical monomer of radius r or a spherocylindrical n-mer of cylindrical radius r and cylindrical length/diameter ratio L_n in a bulk fluid of hard spheres of radius r occupying a total volume fraction ϕ is calculated according to

$$\ln \gamma_{b,n} = \ln(1-\phi) + A_1 Z + A_2 Z^2 + A_3 Z^3, \tag{4}$$

where $A_1 = 7 + 6L_n$, $A_2 = 7.5 + 9L_n$, $A_3 = 3 + 4.5L_n$, $Z = \phi/(1-\phi)$, and $L_n = 2(n-1)/3$ (22,23). Combining Eqs. 3 and 4 leads to

$$\ln K = \ln K_0 + \ln(1-\phi) + 3Z + 1.5Z^2. \tag{5}$$

It follows from Eq. 2 that the concentration of n-mer in the bulk is given by

$$c_{b,n} = K^{n-1}c_{b,1}^n \tag{6}$$

The total concentration of tracer in the bulk fluid is then given by

$$c_{b,tot} = \sum_{n=1}^{\infty} n c_{b,n} = \sum_{i=n}^{\infty} n K^{n-1} c_{b,1}^n. \tag{7}$$

Conversion of Eq. 7 to dimensionless units yields

$$c_{b,tot}^* \equiv K c_{b,tot} = \sum_{n=1}^{\infty} n(Kc_{b,1})^n = \frac{c_{b,1}^*}{\left(1-c_{b,1}^*\right)^2}, \tag{8}$$

where $c_{b,1}^* \equiv Kc_{b,1}$. We define the reference quantity $c_{b,tot}^{*0} \equiv K_0 c_{b,tot}$, which denotes the dimensionless concentration of tracer in the bulk in the absence of crowder. It is this quantity that is held constant when the model calculations described below are performed for varying values of ϕ. It follows from Eq. 5 that

$$\ln c_{b,tot}^*(\phi) = \ln c_{b,tot}^{*0} + \ln(1-\phi) + 3Z + 1.5Z^2. \tag{9}$$

Thus, given the values of $c_{b,tot}^{*0}$ and ϕ, one can calculate the values of all $c_{b,n}^*$ using Eqs. 6, 8, and 9.

Partitioning of tracer n-mer between bulk and surface

The equilibrium between n-mer in the bulk and adsorbed n-mer is given by

$$\ln\frac{c^*_{s,n}}{c^*_{b,n}} = \ln\gamma_{b,n} - \ln\gamma_{s,n} - n\Delta H_{ads}/RT + \Delta S_{ads,n}/R, \quad (10)$$

where $c^*_{s,n}$ denotes the dimensionless concentration of adsorbed n-mer ($\equiv K_0 c_{s,n}$), $\gamma_{s,n}$ is the thermodynamic activity coefficient of adsorbed n-mer, ΔH_{ads} is the enthalpy of adsorption per monomeric subunit, $\Delta S_{ads,n}$ is the change in entropy accompanying adsorption of an n-mer, R is the molar gas constant, and T is the absolute temperature. To simplify the notation, we shall henceforth write ΔH_{ads} in units of RT, and $\Delta S_{ads,n}$ in units of R. In the simplified model presented here, the change in entropy is assumed to be due to a loss in possible rotational configurations:

$$\Delta S_{ads,n} = \ln\left(\Omega^{(rot)}_{s,n}\Big/\Omega^{(rot)}_{b,n}\right), \quad (11)$$

where $\Omega^{(rot)}_{s,n}$ and $\Omega^{(rot)}_{b,n}$ denote the number of rotational configurations accessible to an n-mer in the surface and bulk compartments, respectively. We may estimate the value of $\Delta S_{ads,n}$ as follows: Consider a spherocylinder of diameter $2r$ and cylindrical length $2rL_n$. In the bulk compartment, this spherocylinder may have any orientation. The total number of these orientations is proportional to the surface area of a sphere of radius rL_n. An adsorbed spherocylinder can only have orientations such that the spherocylinder is entirely between two planes separated by a distance $2r(Q-1)$, corresponding to the fraction of the surface area of the sphere of radius rL_n that lies between $\pm\ (Q-1)r$ of the equator. Thus, we may write

$$\Omega^{(rot)}_{b,n} \propto 4\pi(rL_n)^2 \quad (12)$$

and

$$\Omega^{(rot)}_{s,n} \propto 4\pi(rL_n)^2 - 4\pi(rL_n)[rL_n - (Q-1)r]. \quad (13)$$

Combining Eqs. 11–13 yields

$$\Delta S_{ads,n} \approx \begin{cases} 0 & \text{for } n = 1 \\ \ln(Q-1) - \ln L_n & \text{for } n>1 \end{cases}. \quad (14)$$

The calculation of $\ln\gamma_{s,n}$ proceeds in two stages, corresponding to two levels of approximation: two-body and multibody.

Stage 1. Two-body approximation. The two-body approximation was inspired by previous work by Sear (24), who estimated the work required to move a spherocylindrical particle from the interior of a hard-sphere fluid to a hard-wall boundary. Sear treated the excluded volume at the level of two-body interactions, consistent with Asakura-Oosawa theory (25). In a similar fashion, considering only the interaction of tracer with a single crowding particle, we may write (26)

$$\ln\gamma_{b,n} = V_{b,nC}\rho_C \quad (15)$$

and

$$\ln\gamma_{s,n} = V_{s,nC}\rho_C, \quad (16)$$

where ρ_C denotes the number density of hard spherical crowding particles, and $V_{b,nC}$ and $V_{s,nC}$ respectively denote the volume that is excluded to the center of mass of a crowder sphere when a spherocylindrical n-mer is in the interior of the fluid and when it is lying flat against the hard surface. It follows that at this level of approximation,

$$\ln\gamma_{s,n}(\phi) = R_V \ln\gamma_{b,n}(\phi), \quad (17)$$

where $R_V = V_{s,nC}/V_{b,nC}$. The two exclusion volumes are indicated schematically in Fig. 2. It is evident that $R_V \approx 0.5$, independently of n for $Q \approx 1$, as approximately half of the volume excluded by the spherocylinder to the crowder in bulk is already excluded to the crowder particle by the wall (in the absence of the spherocylinder) when the spherocylinder is lying against the wall.

Stage 2. Multibody approximation. The two-body approximation neglects simultaneous interaction between the tracer n-mer and more than one crowder particle. In addition, the approximation assumes that the distribution of

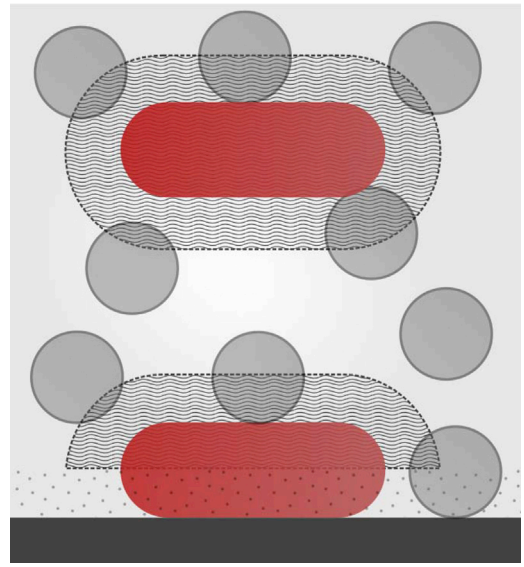

FIGURE 2 Regions shaded with wavy lines indicate the volumes excluded by a spherocylindrical tracer n-mer to a spherical crowder particle in the bulk (*top*) and when adsorbed to the surface (*bottom*). The region shaded with dots in the lower image indicates the volume excluded by the hard wall to a crowder sphere in the absence of adsorbed tracer n-mer. To see this figure in color, go online.

crowder particles in the fluid is independent of position relative to the wall, whereas previous Monte Carlo (MC) studies of a hard-sphere fluid adjacent to a wall indicated that the density of spheres adjacent to the wall is greater than that in the bulk fluid (27,28). Both of these effects become more pronounced with increasing ϕ.

To improve our estimate of ln $\gamma_{s,n}$, we performed MC calculations of the probability of successful insertion of a spherical monomer or a spherocylindrical n-mer into a hard-sphere fluid, as described below. A total of 1024 hard-sphere particles were placed in a cubic simulation box that was periodic in the x and y directions and contained a hard planar wall in the z direction. The sphere diameters were scaled to match the desired packing fraction ϕ, where the value of ϕ ranged from 0.02 to 0.30. Each MC cycle consisted of displacing each sphere a distance of d in a direction chosen uniformly at random. The value of d was adjusted to achieve a 40–60% acceptance ratio. The spheres were initially arranged on the sites of a face-centered cubic lattice. After the optimal value of the displacement distance was determined, the system was run for 10^5 cycles, during which time the initial configuration was lost as the system rapidly equilibrated.

A data collection phase was started after equilibration of the hard sphere fluid. During this phase, a snapshot of the crowder conformation was saved every 10^3 MC cycles for a total of 10^4 times. For each snapshot, we attempted a minimum of 10^4 trial insertions of spheres or spherocylinders of varying lengths representing monomers through tetramers. Each n-mer was inserted at a height z relative to the surface of the hard bounding wall. Spherocylindrical n-mers were oriented randomly in the bulk but oriented nearly parallel to the boundary when placed within the surface compartment, consistent with restrictions of orientation imposed by the value of Q. We determined the probability of a successful insertion of a hard spherical monomer or spherocylindrical n-mer into a fluid of hard spheres (i.e., no overlap of the inserted particle with any hard sphere) by repeating the insertion trials until the ratio of the number of successful insertions to the total number of insertion trials became constant to within 1% of the reported value. In the bulk fluid (distant from the surface), we found no significant difference between the successful insertion probability of a randomly oriented polymer and a polymer constrained to lie parallel to the wall, indicating that our box was sufficiently large.

The results of these calculations are summarized in Fig. 3, in which the natural logarithm of the ratio of the probability of successful insertion of an n-mer into the fluid distant from the surface to the probability of successful insertion of the same n-mer into the fluid adjacent to the surface is plotted as a function of ϕ for monomer, dimer, trimer, and tetramer.

It follows from the Widom insertion theorem (29) that the probability of successful insertion of a hard particle into a

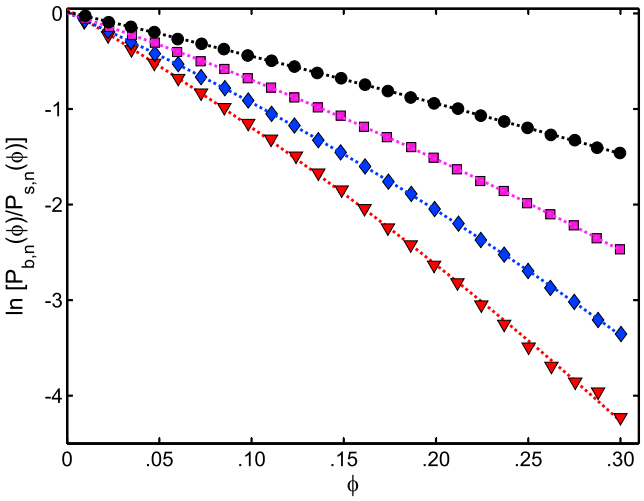

FIGURE 3 MC calculation of the logarithm of the ratio of successful insertion probabilities of an n-mer in the bulk to that at the surface, plotted for monomers (*black circles*), dimers (*magenta squares*), trimers (*blue diamonds*), and tetramers (*red triangles*) as a function of the fraction of volume occupied by crowder. Symbols indicate calculated results, and dashed curves are empirical quadratic functions to guide the eye. To see this figure in color, go online.

fluid of other hard particles is related to the thermodynamic activity coefficient of the inserted particle by

$$\gamma_{x,n}(\phi) \;=\; 1/P_{x,n}(\phi), \tag{18}$$

where $\gamma_{x,n}$ denotes the thermodynamic activity coefficient of the inserted particle in compartment x ($x = b$ for bulk or s for surface), and $P_{x,n}(\phi)$ denotes the probability of successfully inserting an n-mer into this compartment. Combining Eqs. 17 and 18, we obtain

$$R_V(\phi) \;=\; 1 + \ln\left(\frac{P_{b,n}(\phi)}{P_{s,n}(\phi)}\right) \Big/ \ln\,\gamma_{b,n}(\phi), \tag{19}$$

Using Eq. 4 to calculate ln $\gamma_{b,n}(\phi)$, and Eq. 19 together with the ln(ratio) data plotted in Fig. 3, we can calculate the values of $R_V(\phi)$ plotted in Fig. 4. These results confirm two predictions of the first-order treatment described above, namely, that R_V is approximately independent of the length of the oligomer, and the estimated value of $R_V \approx 0.5$ is approximately correct in the limit of low ϕ. However, it is clear that the value of R_V increases significantly with increasing ϕ. This is in accord with our intuition that the local concentration of crowder at the wall increases in proportion to that of the monomeric tracer, since they are the same size, and the local increase in crowder concentration at the wall relative to the bulk will counteract the excluding effect of bulk crowder to some extent, a phenomenon that is neglected in the first-order approximation. We can obtain an analytical approximation to the results plotted in Fig. 4 by fitting a straight line to the plotted data. The best-fit straight line, calculated according to

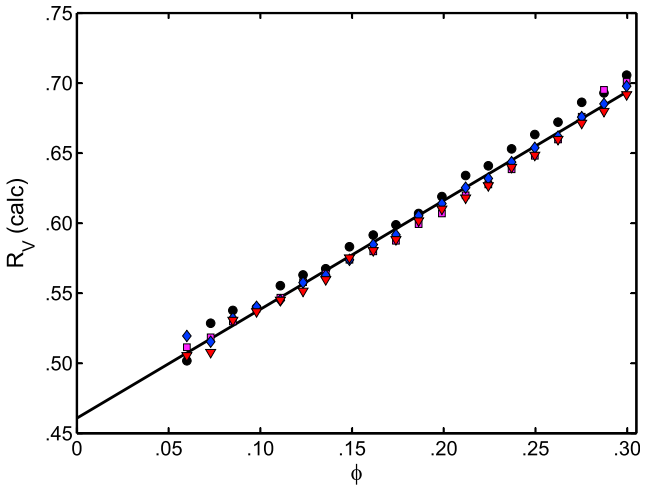

FIGURE 4 Dependence of R_V on ϕ, calculated according to Eq. 19. Symbols correspond to results obtained from insertion probabilities of monomer (*black circles*), dimer (*magenta squares*), trimer (*blue diamonds*), and tetramer (*red triangles*). The calculated points are empirically described by the straight line calculated using values of the intercept and slope given in the text. To see this figure in color, go online.

$$R_V(\phi) = 0.461 + 0.777\phi, \tag{20}$$

is plotted together with the data in Fig. 4. Combining Eqs. 10, 17, and 20, we obtain

$$\ln c^*_{s,n} = \ln c^*_{b,n} + [1 - R_V(\phi)]\ln \gamma_{b,n} - n\Delta H_{ads} + \Delta S_{ads,n}, \tag{21}$$

Given the values of $c^*_{b,n}$ calculated as described in the preceding section, ΔH_{ads}, and Q, the values of $c^*_{s,n}$ are calculated using Eqs. 14, 20, and 21.

Total distribution of tracer

The total concentration of tracer in bulk solution is denoted by $c^*_{b,tot}$ (see Eqs. 7 and 8 above). Since the values of $c^*_{s,n}$ may in principle be calculated for all n, one may in principle sum $nc^*_{s,n}$ over all n to calculate $c^*_{s,tot}$. However, for reasons that will become apparent below, under certain conditions adsorbed oligomers can grow without bound. Therefore, we perform the calculation to a finite maximum value of n, denoted as $n_{\max}$, and demonstrate below that with increasing $n_{\max}$, the system approaches an asymptotically limiting behavior. Thus the total concentration of adsorbed tracer is obtained using

$$c^*_{s,tot} = \sum_{n=1}^{n_{max}} nc^*_{s,n}. \tag{22}$$

The total concentration of tracer in both the bulk and the surface compartment is then given by

$$c^*_{tot} = \left(1 - f_{surface}\right)c^*_{b,tot} + f_{surface}c^*_{s,tot}.$$

The mass fraction of each species of tracer in the bulk and surface compartment may then be calculated according to

$$f_{b,n} = nc^*_{b,n}/c^*_{tot} \tag{23a}$$

and

$$f_{s,n} = nc^*_{s,n}/c^*_{tot}. \tag{23b}$$

It follows that the mass average sizes of tracer in the bulk and surface compartment are given by

$$\langle n\rangle_b = \sum_{n=1}^{\infty} nf_{b,n} \Big/ \sum_{n=1}^{\infty} f_{b,n} \tag{24a}$$

and

$$\langle n\rangle_s = \sum_{n=1}^{n_{max}} nf_{s,n} \Big/ \sum_{n=1}^{n_{max}} f_{s,n}. \tag{24b}$$

Finally, the mass fraction of tracer adsorbed (i.e., in the surface compartment) is given by

$$f_s = \sum_{n=1}^{n_{max}} f_{s,n}. \tag{25}$$

General properties of the model

It follows from the definitions of $f_{b,n}$ and $f_{s,n}$ above that

$$\ln\frac{f_{b,n+1}}{f_{b,n}} = \ln\frac{i+1}{i} + \ln\frac{c^*_{b,n+1}}{c^*_{b,n}} \tag{26a}$$

and

$$\ln\frac{f_{s,n+1}}{f_{s,n}} = \ln\frac{i+1}{i} + \ln\frac{c^*_{s,n+1}}{c^*_{s,n}}. \tag{26b}$$

We define the equilibrium partition coefficient for n-mer as

$$K_P(n) \equiv c^*_{s,n}/c^*_{b,n}. \tag{27}$$

Combining Eqs. 26 and 27, we obtain

$$\ln\frac{f_{s,n+1}}{f_{s,n}} = \ln\frac{i+1}{i} + \ln\frac{K_P(n+1)}{K_P(n)} + \ln\frac{c^*_{b,n+1}}{c^*_{b,n}}. \tag{28}$$

Because tracer in the bulk is defined to self-associate isodesmically,

$$\ln\frac{c^*_{b,n+1}}{c^*_{b,n}} = \ln c^*_{b,1} \tag{29}$$

$$\ln\frac{f_{b,n+1}}{f_{b,n}} = \ln\frac{n+1}{n} + \ln c^*_{b,1}. \tag{30}$$

From Eq. 21, we obtain

$$\ln K_P(n) = -n\Delta H_{ads} + \Delta S_{ads,n} + [1 - R_V(\phi)]\ln \gamma_{b,n} \quad (31)$$

so that

$$\ln \frac{K_P(n+1)}{K_P(n)} = -\Delta H_{ads} + (\Delta S_{ads,n+1} - \Delta S_{ads,n}) + [1 - R_V(\phi)]\left(\ln \gamma_{b,n+1} - \ln \gamma_{b,n}\right). \quad (32)$$

Combining Eqs. 4, 14, 20, and 32, we obtain

$$\ln \frac{K_P(n+1)}{K_P(n)} = -\Delta H_{ads} + \ln \frac{i}{i+1} + [1 - R_V(\phi)] \times (4Z + 6Z^2 + 3Z^3), \quad (33)$$

where $Z \equiv \phi/1 - \phi$. Combining Eqs. 28, 29, and 33, we obtain

$$\ln \frac{f_{s,n+1}}{f_{s,n}} = -\Delta H_{ads} + [1 - R_V(\phi)]\left(4Z + 6Z^2 + 3Z^3\right) + \ln c^*_{b,1}(\phi). \quad (34)$$

RESULTS AND DISCUSSION

In Fig. 5 the calculated values of $\ln(f_{b,n+1}/f_{b,n})^* \equiv \lim_{n\to\infty}[\ln(f_{b,n+1}/f_{b,n})] = c^*_{b,1}$ and $\ln(f_{s,n+1}/f_{s,n})$ are plotted as functions of ϕ for different values of ΔH_{ads} and $\ln c^{*0}_{b,tot}$. Whereas both $\ln(f_{s,n+1}/f_{s,n})$ and $\ln(f_{b,n+1}/f_{b,n})^*$ increase with increasing ϕ, the value of $\ln(f_{b,n+1}/f_{b,n})^*$ always remains negative, indicating that the distribution of oligomeric species in the bulk always remains finite. In contrast, at some value of ϕ, which we call the critical value and denote by ϕ_{crit}, the value of $\ln(f_{s,n+1}/f_{s,n})$ attains a value of zero and becomes positive at greater values, indicating that when $\phi \geq \phi_{crit}$, the distribution of adsorbed oligomer species is unbounded and essentially all tracer is adsorbed. The value of ϕ_{crit} corresponding a particular value of ΔH_{ads} may be obtained by numerical solution of Eq. 34 for ϕ, when the value of $\ln(f_{s,n+1}/f_{s,n})$ is set equal to zero. In Fig. 6 the value of ϕ_{crit} thus calculated is plotted as a function of ΔH_{ads} for two values of $\ln c^{*0}_{b,tot}$. A remarkable feature emerges: the condensation of tracer onto the surface takes place even when $\Delta H_{ads} \geq 0$, that is, in the absence of an intrinsic attractive interaction between the tracer and the surface, and even in the presence of a repulsive tracer-wall interaction. The condensation is clearly driven by the very large crowding-induced difference between $\ln \gamma_{b,n}$ and $\ln \gamma_{s,n}$ (see Eq. 10), which increases strongly with increasing ϕ and n.

One can explore the equilibrium behavior of the system by calculating the dependence of $\langle n\rangle_b, \langle n\rangle_s$ and f_s on ϕ and ΔH_{ads}, as described in the preceding section. The results presented below were calculated using a value of $n_{\max} = 800$ and $Q = 1.05$. Test calculations presented in Fig. S2 of the Supporting Material demonstrate that the equilibrium properties calculated with this value of $n_{\max}$ agree with those expected for the unbounded system to within a very small margin of error, and that variation of Q over a wide range has only a minor quantitative effect, and no qualitative effect, on the behavior of the model.

The calculated dependencies of $\langle n\rangle_b, \langle n\rangle_s$ and f_s on ϕ are plotted in Fig. 7 for several values of ΔH_{ads} and for small and large values of f_{surface}. We call attention to the following qualitative features: At very low levels of crowding, the average size of the adsorbed tracer is smaller than that of the bulk tracer (Fig. 7 *A*). However, as ϕ approaches ϕ_{crit}, the average size of the adsorbed tracer starts to increase sharply, and at ϕ_{crit} it reaches a value of $n_{\max}/2$ (Fig. 7 *B*). The steeply rising value of $\langle n\rangle_s$ as ϕ approaches ϕ_{crit} is

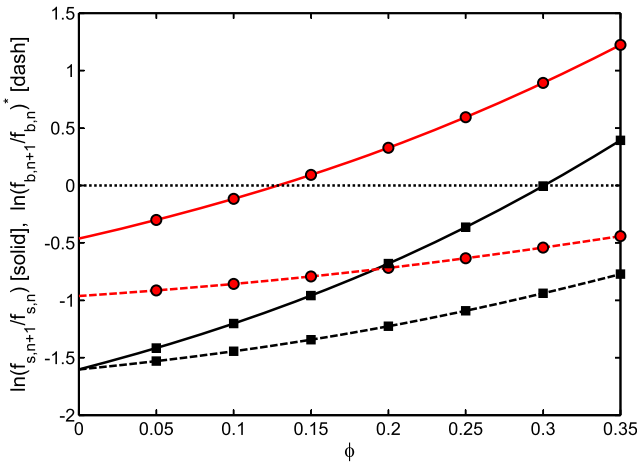

FIGURE 5 Dependence of $\ln(f_{b,n+1}/f_{b,n})^*$ (*dashed curves*) and $\ln(f_{s,n+1}/f_{s,n})$ (*solid curves*) on ϕ, calculated for $\Delta H_{ads} = -.5$, $\ln c^{*0}_{tot} = 0$ (*red circles*) and $\Delta H_{ads} = 0$, $\ln c^{*0}_{tot} = -.5$ (*black squares*). To see this figure in color, go online.

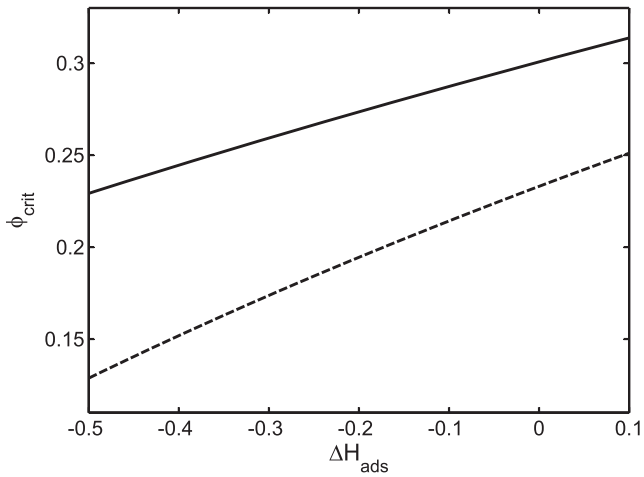

FIGURE 6 Dependence of ϕ_{crit} on ΔH_{ads} calculated for $\ln c^{*0}_{tot} = -0.5$ (*solid curve*) and 0 (*dashed curve*).

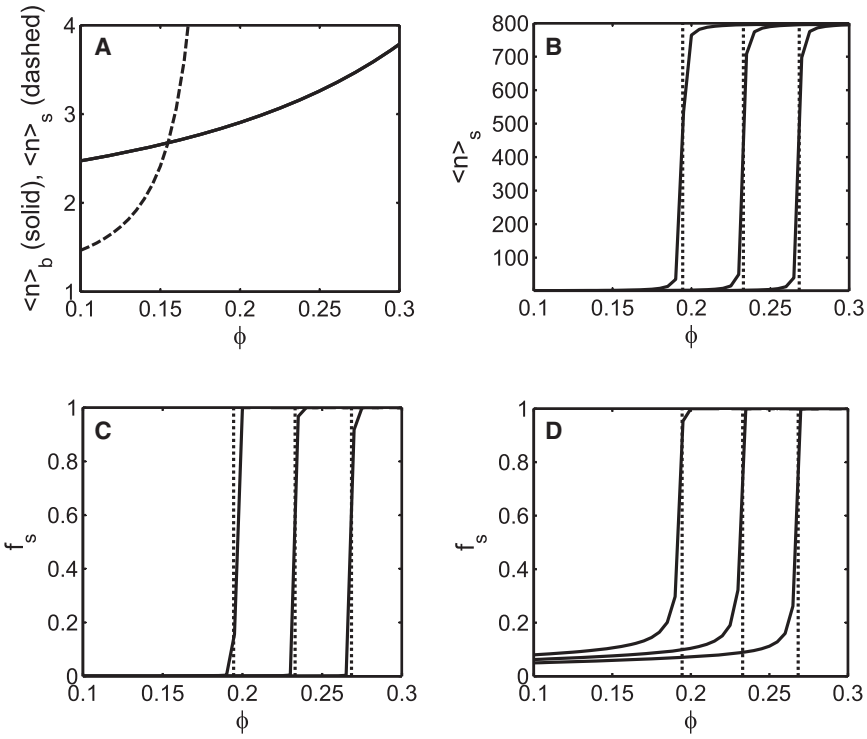

FIGURE 7 Equilibrium properties of the model calculated for $n_{\max} = 800$, plotted as functions of ϕ. Vertical dotted lines indicate values of ϕ_{crit} calculated for the corresponding value of ΔH_{ads}. (*A*) Average size of bulk oligomers. (*B*) Average size of adsorbed oligomers. (*C*) Fraction of tracer adsorbed calculated for $f_{\text{surface}} = 0.001$. (*D*) Fraction of tracer adsorbed calculated for $f_{\text{surface}} = 0.1$. Multiple curves plotted in panels *B–D* correspond to results obtained for $\Delta H_{ads} = -0.2$ (left), 0 (center), and 0.2 (right), respectively.

associated with a concurrent increase in the fraction of tracer that is adsorbed to the surface (Fig. 7, *C* and *D*). For small values of f_{surface} (Fig. 7 *C*), the transition between a slightly oligomerized tracer in bulk and a highly oligomerized adsorbed tracer is highly cooperative, with 99% of the increase in f_s occurring over an increase of just 0.003 in ϕ (cf. Fig. S1). Based on the observation that the steepness of the increases in both $\langle n \rangle_s$ and f_s increases monotonically with increasing $n_{\max}$, and that at ϕ_{crit}, $\langle n \rangle_s$ increases in proportion to $n_{\max}$, both transitions are expected to approach step functions in the limit of large $n_{\max}$. At large values of f_{surface} (Fig. 7 *D*), the amount of tracer that is adsorbed is significant at low values of ϕ and when $\langle n \rangle_s \ll n_{\max}$, although the transition to maximal oligomerization and complete adsorption when $\phi = \phi_{crit}$ is retained. As predicted from an examination of the results in Figs. 6 and 7, the qualitative behavior of the model seems to be unchanged when ΔH_{ads} increases from negative to zero, and even when it becomes positive. Given a sufficiently high degree of crowding, the thermodynamic driving force toward adsorption will ultimately overcome at least a modest intrinsically repulsive interaction between the tracer and the surface.

The calculated dependence of $\langle n \rangle_s$ and f_s on ΔH_{ads} is plotted in Fig. 8 for $\phi = 0.18$ and small and large values of f_{surface}. Just as ϕ_{crit} was defined as the value of ϕ that satisfies Eq. 34 for a given value of ΔH_{ads} and $\ln(f_{s,n+1}/f_{s,n}) = 0$, the quantity $\Delta H_{ads,crit}$ is defined as the value of ΔH_{ads} that satisfies Eq. 34 for a given value of ϕ and $\ln(f_{s,n+1}/f_{s,n}) = 0$. For fixed ϕ and $f_{\text{surface}} \ll 1$, the transitions between maximal and minimal oligomerization and tracer adsorption are sharply dependent on the value of ΔH_{ads}: 95% of the oligomerization of adsorbed oligomer occurs when ΔH_{ads} is decreased by only 0.06 *RT*, and almost 100% of tracer is adsorbed when ΔH_{ads} is decreased by only 0.02 *RT*. As in the case of the dependence of these quantities on ϕ for fixed ΔH_{ads}, the steepness of the transitions increases monotonically with increasing $n_{\max}$ (data not shown), and both transitions are expected to approach step functions in the limit of large $n_{\max}$. It follows from Eq. 34 that if the intrinsic interaction between the tracer and surface becomes sufficiently attractive, the tracer may undergo a highly cooperative transition from being slightly self-associated in solution to highly self-associated on the surface, even in the absence of crowding. This result was hinted at by an earlier analysis (19), but was only fully developed here.

The major qualitative finding of this study is that the combination of excluded-volume effects and adsorption may lead to an extremely cooperative dependence of adsorption and fiber formation on both the volume fraction of the crowder and the magnitude of the intrinsic interaction between the tracer and surface. In the most extreme case, the model predicts that $d\langle n_s \rangle/d\phi$, $df_s/d\phi$, $-d\langle n_s \rangle/d\Delta H_{ads}$, and $-df_s/d\Delta H_{ads}$ will approach ∞ in the limit of large $n_{\max}$, although this limit is unlikely to be reached in any real system. It seems highly likely that the growth of a fiber on the surface will be limited by the occupancy of the surface by other fibers and crowder particles, and also by the increasing probability of fiber fragmentation with increasing fiber length (30,31).

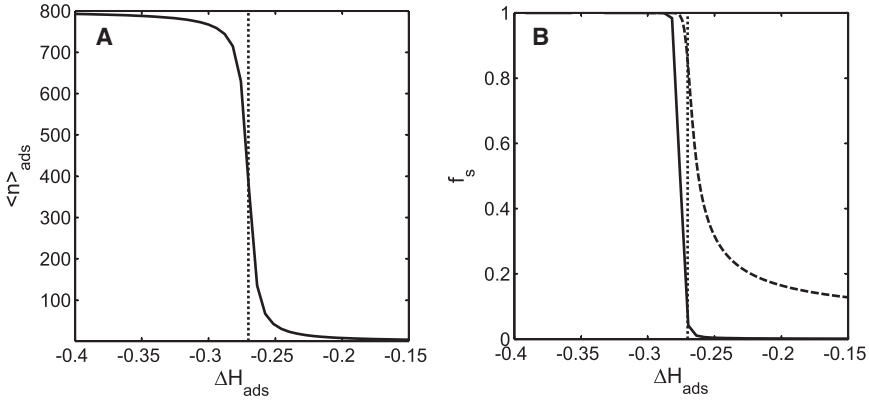

FIGURE 8 Equilibrium properties of model calculated for $n_{max} = 800$, plotted as functions of ΔH_{ads} for $\phi = 0.18$. Vertical dotted lines indicate the value of $\Delta H_{ads,crit}$ for this value of ϕ. (*A*) Average size of adsorbed oligomers. (*B*) Fraction of tracer adsorbed, calculated for $f_{surface} = 0.001$ (*solid curve*) and $f_{surface} = 0.1$ (*dashed curve*).

The model we have presented here contains obvious simplifying approximations, and it is important to inquire whether these simplifications could lead to qualitatively incorrect conclusions. Three examples follow. 1) The representation of proteins and protein aggregates by equivalent hard particles and the use of scaled-particle theory to estimate the thermodynamic activities of these particles is justified by a broad variety of successful predictions and descriptions of the properties of proteins in a highly nonideal solution (for specific examples, see citations in Hall and Minton (15), Zhou et al. (16), and Zimmerman and Minton (17)). 2) It was correctly pointed out by a reviewer that in a system containing a real protein in a real aqueous solvent, in contrast to our simplified hard-particle protein model, the quantity we have denoted by ΔH_{ads} might not be entirely enthalpic, as it could include contributions from hydrophobic interactions between the tracer and surface, which are partially entropic in nature. However, the distinction is inconsequential in this context since the analysis is confined to constant temperature. 3) The assumption that the self-association of the tracer in the bulk is isodesmic is clearly an approximation. However, a previous theoretical analysis indicated that significant deviations from a constant stepwise free energy of addition are limited to oligomer sizes smaller than five (32), and our calculations extend to oligomer sizes of several hundred. Moreover, the experimentally measured linear self-association of several proteins in solution has been quantitatively accounted for by isodesmic or quasi-isodesmic models (3,33), indicating either that stepwise entropy changes are less sensitive to oligomer length than predicted by idealized rigid-rod models or that the enthalpic contribution to the total free energy of stepwise addition of monomer to oligomer far outweighs the entropic contribution, Clearly, the model presented here could be expanded in a number of directions, including more general and perhaps more realistic definitions of tracer-wall interaction and tracer self-association. However, it is by no means obvious that the increased complexity associated with generalization would provide additional qualitative insight.

It should be kept in mind that the model presented here is an equilibrium model and does not in and of itself predict either the primary reaction pathways or the rate at which equilibrium will be attained. However, it is clear that in a crowded system, the presence of large fibers in solution is highly thermodynamically disfavored. Moreover, the adsorption of long fibers requires translation and rotation via diffusional processes that would be extremely slow in dilute solution (34) and substantially slower in a crowded medium (23,35). Thus, we expect fibrillation to proceed primarily via the migration of tracer monomers and small oligomers to the surface, and the subsequent growth of fibers on the surface to proceed by addition of tracer monomer to the ends of adsorbed fibers. The rates of tracer monomer diffusion to the surface, subsequent adsorption, and migration on the surface depend on the packing fractions of crowder in the bulk and surface compartments, and the relative strength of the tracer-wall interaction. Depending on the relative magnitude of the effect of each of these three factors, either the migration of monomer to the surface or the rate of addition of adsorbed monomer to adsorbed fiber, or a combination of both, could be rate limiting.

CONCLUSIONS

Semi-empirical theories regarding the effect of crowding on translational diffusion of globular particles in three- and two-dimensional fluids (23,36,37) predict a reduction in the translational diffusional coefficient of monomer of $<$10-fold at the highest volume fractions of crowder considered in this work. The effect of crowding on the rotational diffusion of globular proteins is expected to be smaller (38). Thus, we expect that the highly (and possibly uniquely) cooperative transition from low-molecular-weight soluble tracer to high-molecular-weight adsorbed tracer predicted by our model will be experimentally observable, provided that a suitable combination of tracer species, crowder species, and surface can be found. The criteria for suitability are that 1) the tracer species can be shown to form linear fibrils of indefinite length by means of an isodesmic or quasi-isodesmic association scheme; 2) the tracer species and

surface can be shown to exhibit a reversible interaction that can be modulated by varying experimental variables such as the pH, salt concentration, and temperature; and 3) the crowder species, of size comparable to that of the monomeric tracer, can be shown to be inert (or nearly so) with respect to both the tracer and the surface.

SUPPORTING MATERIAL

Two figures are available at http://www.biophysj.org/biophysj/supplemental/S0006-3495(14)04811-5.

AUTHOR CONTRIBUTIONS

T.H. designed the model, performed MC simulations, and wrote the article. A.P.M. designed the model, performed equilibrium calculations, and wrote the article.

ACKNOWLEDGMENTS

The authors thank the anonymous reviewers for incisive and helpful comments.

This research was supported by the Intramural Research Division of the National Institute of Diabetes and Digestive and Kidney Diseases, NIH. This study utilized the high-performance computational capabilities of the Biowulf Linux cluster at the National Institutes of Health, Bethesda, MD. (http://biowulf.nih.gov).

REFERENCES

1. Díaz, J. F., M. Menéndez, and J. M. Andreu. 1993. Thermodynamics of ligand-induced assembly of tubulin. *Biochemistry.* 32:10067–10077.
2. Korn, E. D., M. F. Carlier, and D. Pantaloni. 1987. Actin polymerization and ATP hydrolysis. *Science.* 238:638–644.
3. Rivas, G., A. López, …, J. M. Andreu. 2000. Magnesium-induced linear self-association of the FtsZ bacterial cell division protein monomer. The primary steps for FtsZ assembly. *J. Biol. Chem.* 275:11740–11749.
4. Hill, T. L. 1987. Linear Aggregation Theory in Cell Biology. Springer-Verlag, Berlin.
5. Oosawa, F., and M. Kasai. 1962. A theory of linear and helical aggregations of macromolecules. *J. Mol. Biol.* 4:10–21.
6. Pollard, T. D. 1983. Measurement of rate constants for actin filament elongation in solution. *Anal. Biochem.* 134:406–412.
7. Engelborghs, Y., L. C. De Maeyer, and N. Overbergh. 1977. A kinetic analysis of the assembly of microtubules in vitro. *FEBS Lett.* 80:81–85.
8. Frigon, R. P., and S. N. Timasheff. 1975. Magnesium-induced self-association of calf brain tubulin. I. Stoichiometry. *Biochemistry.* 14: 4559–4566.
9. Kasai, M., E. Nakano, and F. Oosawa. 1965. Polymerization of actin free from nucleotides and divalent cations. *Biochim. Biophys. Acta.* 94:494–503.
10. Knull, H., and A. P. Minton. 1996. Structure within eukaryotic cytoplasm and its relationship to glycolytic metabolism. *Cell Biochem. Funct.* 14:237–248.
11. Minton, A. P. 1990. Holobiochemistry: an integrated approach to the understanding of biochemical mechanisms that emerges from the study of proteins and protein associations in volume-occupied solutions. *In* Structural and Organizational Aspects of Metabolic Regulation. P. A. Srere, M. E. Jones, and C. K. Mathews, editors. Wiley-Liss, New York, pp. 291–306.
12. Hall, D., and A. P. Minton. 2002. Effects of inert volume-excluding macromolecules on protein fiber formation. I. Equilibrium models. *Biophys. Chem.* 98:93–104.
13. Hatters, D. M., A. P. Minton, and G. J. Howlett. 2002. Macromolecular crowding accelerates amyloid formation by human apolipoprotein C-II. *J. Biol. Chem.* 277:7824–7830.
14. Rivas, G., J. A. Fernández, and A. P. Minton. 2001. Direct observation of the enhancement of noncooperative protein self-assembly by macromolecular crowding: indefinite linear self-association of bacterial cell division protein FtsZ. *Proc. Natl. Acad. Sci. USA.* 98:3150–3155.
15. Hall, D., and A. P. Minton. 2003. Macromolecular crowding: qualitative and semiquantitative successes, quantitative challenges. *Biochim. Biophys. Acta.* 1649:127–139.
16. Zhou, H.-X., G. Rivas, and A. P. Minton. 2008. Macromolecular crowding and confinement: biochemical, biophysical, and potential physiological consequences. *Annu. Rev. Biophys.* 37:375–397.
17. Zimmerman, S. B., and A. P. Minton. 1993. Macromolecular crowding: biochemical, biophysical, and physiological consequences. *Annu. Rev. Biophys. Biomol. Struct.* 22:27–65.
18. Knight, J. D., J. A. Hebda, and A. D. Miranker. 2006. Conserved and cooperative assembly of membrane-bound alpha-helical states of islet amyloid polypeptide. *Biochemistry.* 45:9496–9508.
19. Minton, A. P. 1995. Confinement as a determinant of macromolecular structure and reactivity. II. Effects of weakly attractive interactions between confined macrosolutes and confining structures. *Biophys. J.* 68:1311–1322.
20. Sasahara, K., K. Morigaki, and K. Shinya. 2014. Amyloid aggregation and deposition of human islet amyloid polypeptide at membrane interfaces. *FEBS J.* 281:2597–2612.
21. Stafford, 3rd, W. F., and D. A. Yphantis. 1972. Virial expansions for ideal self-associating systems. *Biophys. J.* 12:1359–1365.
22. Cotter, M. A. 1977. Hard spherocylinders in an anisotropic mean field: a simple model for a nematic liquid crystal. *J. Chem. Phys.* 66:1098–1106.
23. Han, J., and J. Herzfeld. 1993. Macromolecular diffusion in crowded solutions. *Biophys. J.* 65:1155–1161.
24. Sear, R. P. 1998. Depletion driven adsorption of colloidal rods onto a hard wall. *Phys. Rev. E Stat. Phys. Plasmas Fluids Relat. Interdiscip. Topics.* 57:1983–1989.
25. Asakura, S., and F. Oosawa. 1958. Interaction between particles suspended in solutions of macromolecules. *J. Polym. Sci.* 33:183–192.
26. Minton, A. P. 1998. Molecular crowding: analysis of effects of high concentrations of inert cosolutes on biochemical equilibria and rates in terms of volume exclusion. *Methods Enzymol.* 295:127–149.
27. Siderius, D. W., and D. S. Corti. 2005. Extension of scaled particle theory to inhomogeneous hard particle fluids. I. Cavity growth at a hard wall. *Phys. Rev. E Stat. Nonlin. Soft Matter Phys.* 71 (3 Pt 2A):036141.
28. Snook, I. K., and D. Henderson. 1978. Monte-Carlo study of a hard-sphere fluid near a hard wall. *J. Chem. Phys.* 68:2134–2139.
29. Widom, B. 1963. Some topics in the theory of fluids. *J. Chem. Phys.* 39:2808.
30. Hall, D., and H. Edskes. 2009. A model of amyloid's role in disease based on fibril fracture. *Biophys. Chem.* 145:17–28.
31. Knowles, T. P. J., C. A. Waudby, …, C. M. Dobson. 2009. An analytical solution to the kinetics of breakable filament assembly. *Science.* 326:1533–1537.
32. Chatelier, R. C. 1987. Indefinite isoenthalpic self-association of solute molecules. *Biophys. Chem.* 28:121–128.
33. Attri, A. K., C. Fernández, and A. P. Minton. 2010. Self-association of Zn-insulin at neutral pH: investigation by concentration gradient—static and dynamic light scattering. *Biophys. Chem.* 148:23–27.

34. Cantor, C. R., and P. R. Schimmel. 1980. Biophysical Chemistry. Part II. Techniques for the Study of Biological Structure and Function. Freeman, San Francisco.

35. Weiss, M. 2014. Crowding, diffusion, and biochemical reactions. *Int. Rev. Cell. Mol. Biol.* 307:383–417.

36. Minton, A. P. 1989. Lateral diffusion of membrane proteins in protein-rich membranes. A simple hard particle model for concentration dependence of the two-dimensional diffusion coefficient. *Biophys. J.* 55: 805–808.

37. Muramatsu, N., and A. P. Minton. 1988. Tracer diffusion of globular proteins in concentrated protein solutions. *Proc. Natl. Acad. Sci. USA*. 85:2984–2988.

38. Laurent, T. C., and B. Obrink. 1972. On the restriction of the rotational diffusion of proteins in polymer networks. *Eur. J. Biochem.* 28:94–101.